

EFFECT OF INTERPHASE THICKNESS ON TENSILE PROPERTIES OF HI-NICALON™ TYPE-S FCVI COMPOSITES—Y. Katoh, L. L. Snead, and T. Nozawa (Oak Ridge National Laboratory), T. Hinoki and A. Kohyama (Kyoto University), N. Igawa and T. Taguchi (Japan Atomic Energy Research Institute)

OBJECTIVE

The objective of this work is to determine the influence of interphase thickness on tensile properties of the Hi-Nicalon™ Type-S / pyrolytic carbon interphase / chemically vapor infiltrated SiC composite system, in search of the optimum interphase for the near-stoichiometric SiC fiber-reinforced rigid SiC matrix composites for fusion applications.

SUMMARY

Fast fracture properties of chemically vapor-infiltrated silicon carbide matrix composites with Hi-Nicalon™ Type-S near-stoichiometric silicon carbide fiber reinforcements and thin pyrolytic carbon interphase were studied. The primary emphasis was on preliminary assessment of the applicability of a very thin pyrolytic carbon interphase between fibers and matrices of silicon carbide composites for use in nuclear environments. It appears that the mechanical properties of the present composite system are not subject to strong interphase thickness effects, in contrast to those in conventional non-stoichiometric silicon carbide-based fiber composites. The interphase thickness effects are discussed from the viewpoints of residual thermal stress, fiber damage, and interfacial friction. A preliminary conclusion is that a thin pyrolytic carbon interphase is beneficial for fast fracture properties of stoichiometric silicon carbide composites.

PROGRESS AND STATUS

Introduction

Silicon carbide (SiC) is a unique material that maintains high strength and corrosion resistance at temperatures well beyond the typical high temperature limits for superalloys. More importantly, the excellent thermo-mechanical properties of SiC are maintained after neutron irradiation to medium-to-high fluences at elevated temperatures [1]. Continuous SiC fiber-reinforced SiC matrix composites (SiC/SiC composites) can be used as structural materials, since they possess pseudo-ductile, predictable, and tailorable fracture properties in addition to the unique merits of monolithic SiC [2]. Early generations of SiC/SiC composites failed to demonstrate neutron tolerance due to a rapid irradiation-induced densification of 'SiC-based' non-stoichiometric fibers [3–5]. However, as improved SiC fibers became available, experiments started to demonstrate good tolerance of SiC/SiC composites to neutron irradiation [5–7]. Those SiC fibers, which consist primarily of a polycrystalline form of cubic SiC and are termed Generation-III SiC fibers [8], are now commercially available as Hi-Nicalon™ Type-S (Nippon Carbon Co., Tokyo, Japan) [9] and Tyranno™-SA (Ube Industries, Ltd., Ube, Japan) [10]. The Generation-III SiC fiber composites are also considered for application as in-core components of advanced gas thermal reactors [11] and gas fast reactors [12]. Fusion power reactor design studies assume that SiC/SiC composites can be used in gas-cooled solid-breeding blankets [13–16] and helium/Pb-Li dual-coolant blankets [17,18]. Some of the dual-coolant blanket concepts, including the U.S.-proposed Test Blanket Module (TBM) for

the International Thermonuclear Experimental Reactor (ITER), utilize channel inserts made of SiC or SiC/SiC as an electrical and thermal insulator [19].

Among various processing techniques for matrix densification of SiC/SiC composites, chemical vapor infiltration (CVI) is the technique that produces reference materials for nuclear applications [8]. The CVI process is essentially a chemical vapor deposition (CVD) of the matrix material on (coated) fiber surfaces as the substrate. A high purity, stoichiometric, and polycrystalline matrix for SiC/SiC composites can not be efficiently produced by any other industrialized processes. Non-stoichiometric and/or nano-crystalline SiC matrices in melt-infiltrated or polymer-impregnated and pyrolyzed composites are usually prone to deteriorate during irradiation [20,21]. The CVI process is not only effective in producing high strength composites for primary structure applications but is also appropriate for tailoring of trans-thickness thermal and electrical conductivity for the channel insert application, by controlling porosity and inter-fiber spacing.

Another advantage of the CVI technique is that the deposition of fiber-matrix interphases as a CVD coating on the fibers can be incorporated in the matrix densification process. Properties of the interphases are highly tailorable in CVI SiC/SiC composites [22].

The objective of this work is to evaluate the non-irradiated mechanical properties of Generation III SiC fiber-reinforced CVI SiC-matrix composites with a tailored pyrolytic carbon (PyC) interphase. The primary focus was on the influence of interphase thickness, which is a key parameter that controls mechanical properties of ceramic composites. For conventional CVI-SiC/SiC composite systems, an optimum PyC interphase thickness range of 150–300nm is reported for the best fracture behavior [23–26]. However, for application in fusion blankets, the minimum use of carbon constituents is preferred to optimize irradiation stability, chemical compatibility with coolants and/or breeding materials, tritium permeability, and electrical conductivity. The Generation III SiC fibers are significantly different from conventional SiC fibers in physical (coefficient of thermal expansion, elastic modulus), mechanical (fracture strain), chemical (reactivity and bonding at the surface), and topographical (surface roughness) properties. These differences can cause difference in the effect of interphase characteristics on composite properties, so the effects must be quantified.

Experimental Details

The materials studied were Hi-Nicalon™ Type-S fiber-reinforced, PyC interphase, CVI SiC-matrix (Hi-Nicalon Type-S/PyC/CVI-SiC) composites produced at Oak Ridge National Laboratory. Composites with three PyC interphase thicknesses were produced with 2D plain-weave fabric from an early lot of Hi-Nicalon Type-S fibers (Lot# 298201, produced in 1998) with a [0°/30°/60°] stacking sequence ('0/30/60', hereafter) [27]. The average interphase thicknesses were 80, 130, and 270nm. Additionally, one composite was produced with 2D plain-weave fabric of a newer lot of fibers (Lot# 320203, 2002) using a [0°/90°] stacking sequence ('0/90'). The newer Hi-Nicalon Type-S fibers were produced by continuous factory line, including spinning, electron beam curing, and decarbonization, while the older fibers had been produced through a series of batch processes. The specification sheet provided by the manufacturer shows that the newer fibers possess slightly higher nominal tensile strength and very slightly lower tensile modulus than the older fibers. The property differences between the two generations

of Hi-Nicalon Type-S fibers are seen in Table 1, along with the summary of properties of the composites fabricated in this study.

The interphase deposition and matrix densification were carried out in isothermal and temperature gradient [28,29] configurations, respectively, at the High Temperature Materials Laboratory, Oak Ridge National Laboratory (ORNL). Stacks of ~60 fabric sheets of 76 mm-diameters were tightly held in graphite fixtures during the infiltration. The PyC interphase was deposited from propylene precursor ($50 \text{ cm}^3/\text{min}$) diluted with argon ($1000 \text{ cm}^3/\text{min}$) at 1373K and 5kPa total pressure. The interphase thickness was controlled by adjusting the time of deposition, since the deposition rate was fairly constant during the coating process. The SiC matrix was infiltrated using methyltrichlorosilane (MTS, Gelest Inc., Morrisville, PA) at a hot surface temperature of 1373–1473K and back pressure of 100kPa. The liquid MTS precursor was carried by hydrogen bubbled through it at a flow rate of 0.3–0.5 g/min. The deposition rate was approximately 30nm/min.

Tensile specimens were machined from the composite discs with the longitudinal direction parallel to one of the fiber directions. Miniature tensile specimen geometry that had been developed for neutron irradiation studies of ceramic composites was employed [30]. The specimen geometry and dimensions are given in Fig. 1. The gauge length of 15mm and the width of 3mm (corresponding to two thread intervals) are within a range where a systematic gauge size effect is observed [31]. The gauge thickness of ~2.3mm accommodates approximately 10 fabric layers. The tensile testing procedure followed general guidelines of ASTM standards C1275-00 and C1359-96. The tensile test incorporated several unloading / reloading sequences in order to allow analysis on the hysteretic response. For the tests at room temperature (RT), the specimens were clamped by wedge grips with aluminum tabs on both faces of the grip sections. The strain was determined by averaging the readings of strain gauges fastened to both faces of the central gauge section during the testing at RT. The elevated temperature tests were performed at 1573K in a flow of commercial ultra-high purity argon. Edge-loaded passive grips recommended in ASTM standard C1359-96 were employed to hold the specimen. The strain was measured on one side of the gauge section by means of reflective laser extensometry. Details of the elevated temperature testing can be found elsewhere [32]. The crosshead displacement rate was 0.5mm/min for all tests. Fracture surfaces were examined using a field emission scanning electron microscope (FE-SEM).

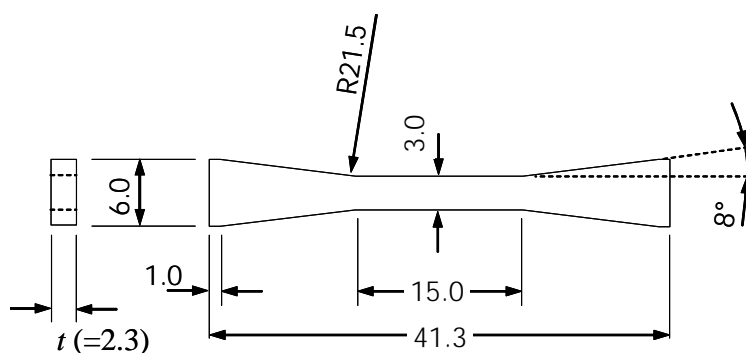


Fig. 1. Geometry of the miniature tensile specimen. Unit of dimensions is millimeter.

Results

The dimensions of the infiltrated composites were 76mm diameter x ~12.7mm thickness. Variations in the interphase coating thickness and porosity within individual discs were both typically $\pm 30\%$. The interphase thickness was determined by microscopic examination on the polished surfaces using an FE-SEM. Examples of backscattered electron images of the composites with the nominal interphase thickness of 80, 130, and 270nm are presented in Fig. 2. The porosity was calculated based on the measured apparent mass density (= mass / envelope volume), measured interphase thickness, and the estimated fiber volume fraction. Because of the significant variations within the nominally identical materials, both the interphase thickness and the porosity were measured for individual mechanical property specimens. Values summarized in Table 1 are those averaged over the tested tensile specimens. The tensile stress – strain curves obtained at RT for the 0/30/60 composites with three different interphase thicknesses are shown in Fig. 3. Each of the curves contains an initial proportional segment that roughly corresponds to the elastic deformation, followed by a second linear portion during which matrix cracks are progressively developing, and a further non-linear portion due to domination of the fiber failure. Although these three specimens failed at similar stress levels, a distinct difference in the fracture strain and in the hysteresis behavior is noted between the composite with 56nm-thick interphase and those with 178 or 315nm-thick interphases.

Figure 4 compares the tensile behavior of the 0/90 composites with thin (43 and 62nm) PyC interphase at RT and at 1573K. The 0/90 composite exhibited significantly higher strength and larger fracture strain than the 0/30/60 composite that have similar interphase thickness. The tensile behavior at 1573K is apparently different from that at RT. However, since the unloading / reloading moduli for unloading from 75, 100, and 125MPa are almost identical, increase in the matrix crack density is not primarily responsible for the increase in permanent strain. Furthermore, the intersection of unloading and reloading segments at higher stress levels suggests that an artificial drift in the test instrumentation is added to the strain reading. Therefore, the elevated temperature data were used only for comparison of the ultimate strength and the matrix damage parameter.

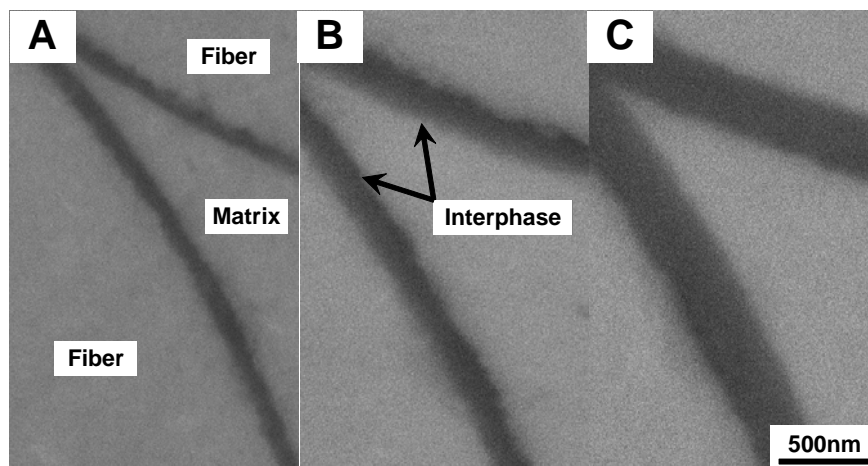


Fig. 2. Backscattered scanning electron images of fiber-matrix interfacial regions of the composites. (A) CVI-1258, $40 < t_{PyC} < 90\text{nm}$, (B) CVI-1257, $150 < t_{PyC} < 180\text{nm}$, (C) CVI-1259, $200 < t_{PyC} < 390\text{nm}$.

An example RT stress – strain curve for Tyranno™-SA SiC-fiber composite, obtained from a companion work [33] is included in Fig. 4. The Tyranno-SA composite has a 2D plain-weave architecture with a thin (25nm) PyC interphase. While the Tyranno-SA and the Hi-Nicalon Type-S composites exhibited similar proportional limit stresses (PLSs) and similar second-stage linear behavior, a major difference is noted in that the Hi-Nicalon Type-S composite failed after matrix crack saturation had been achieved. Additionally, the transition from the proportional to the second linear deformation stage seems to be smoother in the Hi-Nicalon Type-S Composite.

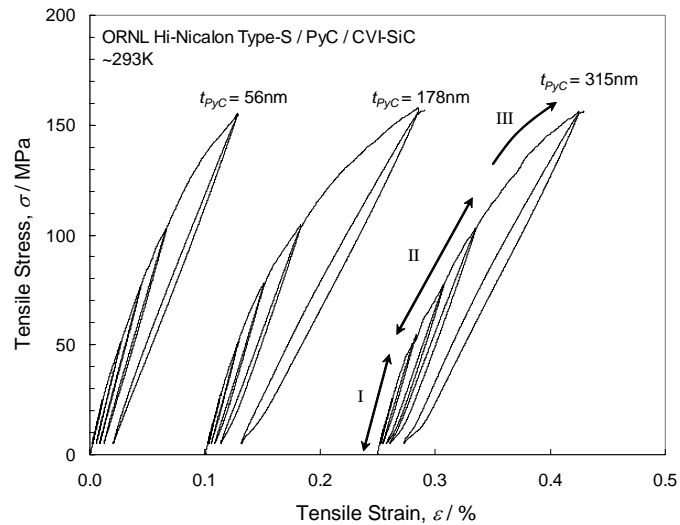


Fig. 3. Representative load – strain curves obtained for Hi-Nicalon™ Type-S (2D-PW, 0°/30°/60°) / PyC / CVI-SiC composites with various PyC interphase thickness. Stages I, II, and III indicate the initial proportional stage, the second linear stage, and the non-linear fiber failure stage, respectively.

The ultimate tensile strength (UTS), PLS, and tensile modulus of the Hi-Nicalon Type-S / PyC / CVI-SiC composites are plotted against the PyC interphase thickness in Figs. 5, 6, and 7, respectively. The PLS was defined as the stress at 5% deviation from the extrapolated linear segment used for the modulus determination. As seen in Fig. 5, the UTS exhibited a slight positive dependence on the interphase thickness, although the dependence might not be statistically significant. No significant difference was shown in UTS, after values were normalized to the longitudinal fiber volume fraction, between the plain-weave 0/30/60 composite and the plain-weave 0/90 composite. The UTS at 1573K appeared lower than that at RT by 10 to 30%.

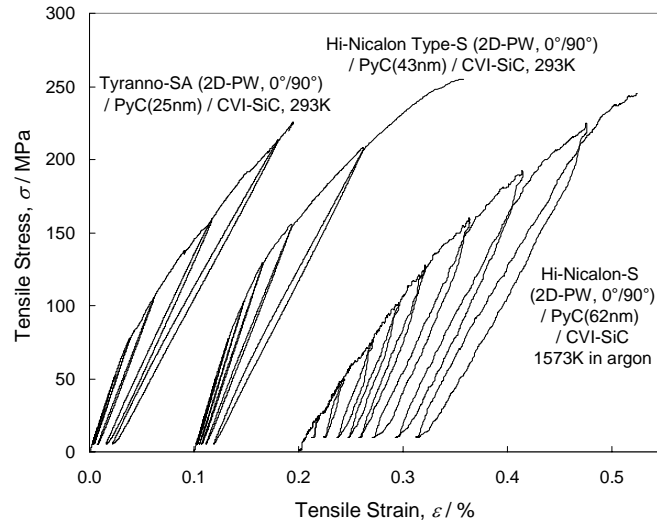


Fig. 4. Comparison of load – strain curves obtained for very thin PyC-interphase Tyranno™-SA composite at room temperature and Hi-Nicalon™ Type-S composite at room temperature and at 1573K in argon.

In contrast to the UTS, the tensile PLS exhibited a negative correlation with the interphase thickness, as shown in Fig. 6. The correlation is significant in this case, as the PLS of 30~40MPa at the interphase

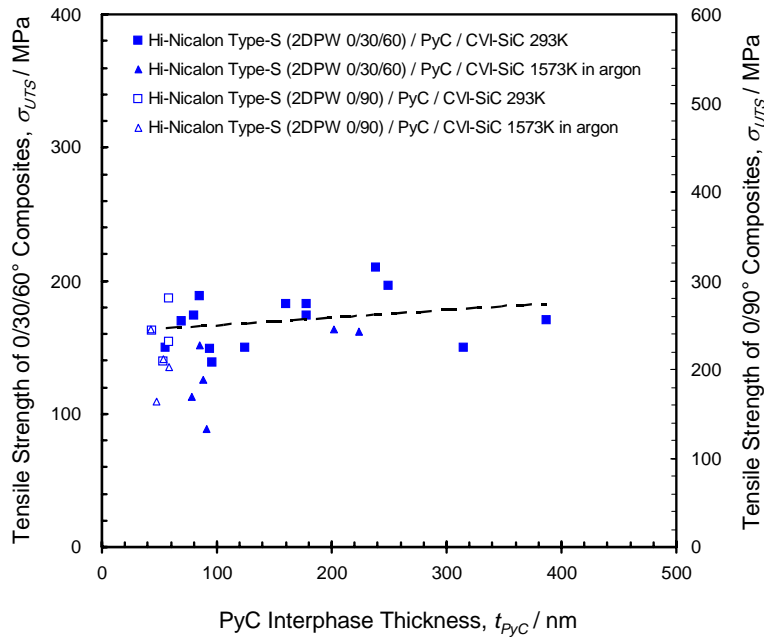


Fig. 5. Ultimate tensile stress of Hi-Nicalon™ Type-S / PyC / CVI-SiC composites at room temperature plotted against PyC interphase thickness

thickness of <100nm decreases to 20~30MPa at >300nm. The plain-weave 0/90 composite exhibited much higher PLS than the plain-weave 0/30/60 composites for similar interphase thickness, even after normalization to the longitudinal fiber fraction. The difference is due most likely to the difference in stacking sequence, since Tyranno-SA 2D-plain weave 0/90 composites with similar interphase features exhibited substantially higher PLS for identical testing condition [33] The PLS could also be affected by the matrix density, but in this case the difference could not be the effect of matrix density, because the porosity in the 0/30/60 composite with interphase thickness <100nm and that in the 0/90 composite are about the same. The influence of 2D fabric architecture on PLS is not known.

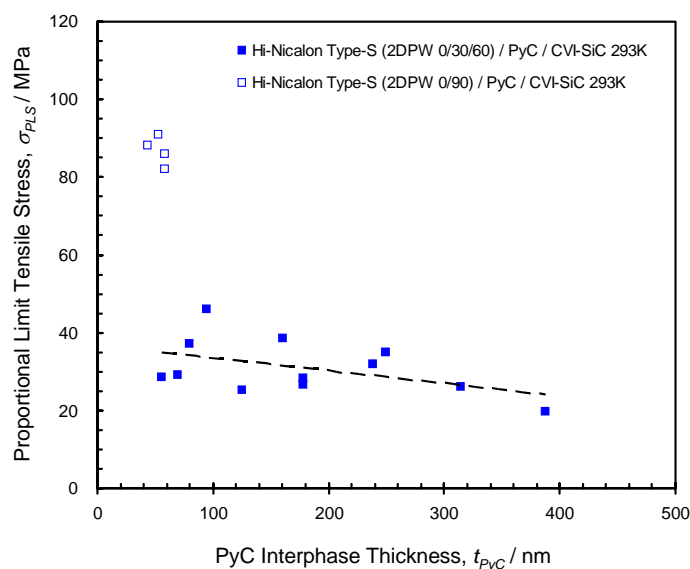


Fig. 6. Proportional limit tensile stress of Hi-Nicalon™ Type-S / PyC / CVI-SiC composites at ambient temperature plotted against PyC interphase thickness.

The tensile tangent modulus was also slightly affected by the interphase thickness. As shown in Fig. 7, the modulus decreases monotonically as the interphase gets thicker. The PyC interphase in these composites consists of near-isotropic glassy carbon. The observed interphase thickness effect on the modulus is primarily a volume effect of the very much less rigid glassy carbon in the rigid silicon carbide. Fitting to a simple model suggests ~10GPa of interphase Young's modulus and ~240GPa of Young's modulus for effective mean medium representing all the other composite constituents including pores [33].

In Figs. 8(A) and (B), typical RT fracture surfaces within the longitudinal fiber bundle regions are compared between composites with 56nm- and 315nm-thick interphases. A substantial population of fibers exhibit pull-out length of 10–30 μ m for the case of 56nm-thick interphase, whereas similar fiber populations could not be identified in the 315nm-thick interphase composite. The rest of the fibers showed pull-out length of ~100 μ m or longer. Pairs of representative fracture surfaces of individual fibers are included as subsets in Fig. 8. Fracture origins in the fibers were identified either on the surface (left) or as an internal flaw (right). Frequencies of fractures originating from surface and from an internal flaw were roughly comparable, although a statistical comparison was not made. A fracture surface of the 44nm-thick interphase composite tested at 1573K is presented in Fig. 8(C). The fiber pull-out length at 1573K appeared substantially longer and was typically 200–300 μ m. The majority of the fibers fractured at the

elevated temperature appeared to have initiated at the surface. It is not known if it is due to an effect of testing temperature or differences between fibers of the two generations.

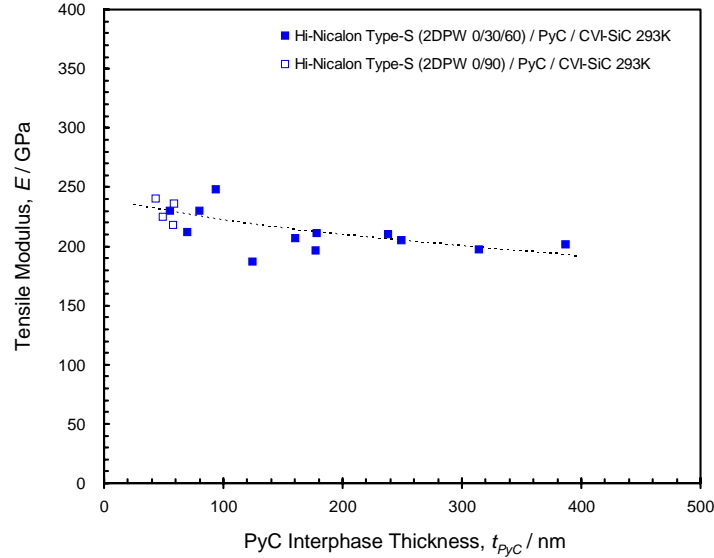


Fig. 7. Influence of PyC interphase thickness on initial tangential modulus of Hi-Nicalon™ Type-S / PyC / CVI-SiC composites.

Discussion

Observations described in the previous section imply that the non-linear tensile behavior could be significantly different between the Hi-Nicalon Type-S composites with PyC interphase $< \sim 100\text{nm}$ or $> \sim 100\text{nm}$. In contrast, the UTS and modulus exhibited small or negligible dependence on the interphase thickness. The relatively small width of the hysteresis loop for the 56nm-thick interphase composite in Fig. 3 indicates the stronger friction at the sliding interfaces, if the matrix crack density is the same [34]. The shorter average fiber pull-out length on the fracture surface of the same composite indicates the stronger friction, since the pull-out length is inversely proportional to the frictional stress [35]. The larger PLS for thinner interphase might be due partly to the stronger friction, according to the model proposed by Curtin for uni-directional composites [35]. However, it could be more closely related to the higher composite modulus, since a substantial fraction of macroscopic cracks in 2D composites initiate at internal pore surfaces [36].

(1) Matrix damage evolution and in-situ fiber strength

The evolution of matrix damage parameters in four different composites with increasing peak tensile stress is plotted in Fig. 9. The matrix damage parameter was defined as:

$$D = 1 - E^* / E_c \quad (1)$$

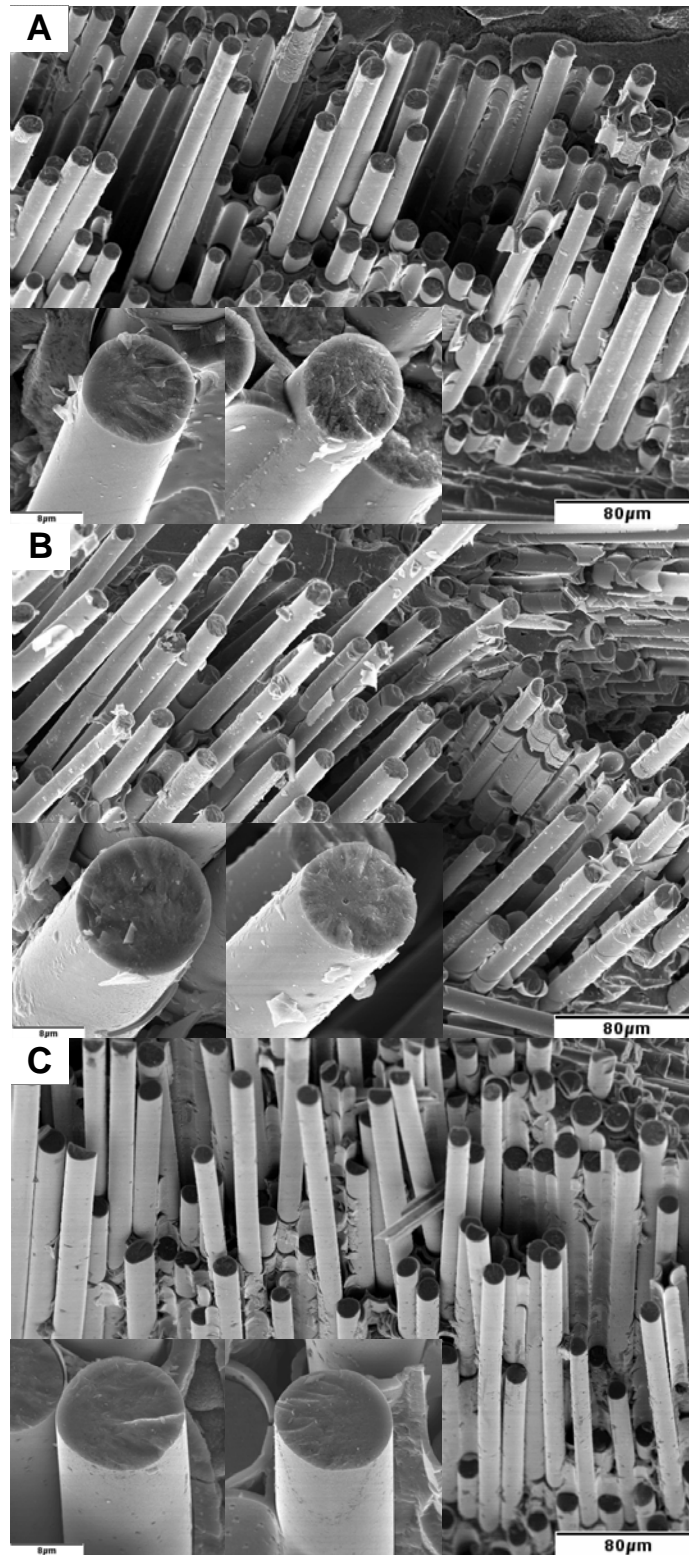


Fig. 8. Longitudinal fiber bundle regions in fracture surfaces of Hi-Nicalon™ Type-S / PyC / CVI-SiC composites. (A) $t_{\text{PyC}}=56\text{nm}$, tested at RT, (B) $t_{\text{PyC}}=315\text{nm}$, tested at RT, and (C) $t_{\text{PyC}}=44\text{nm}$, tested at 1573K in argon. Fiber fracture surfaces are shown in inserts.

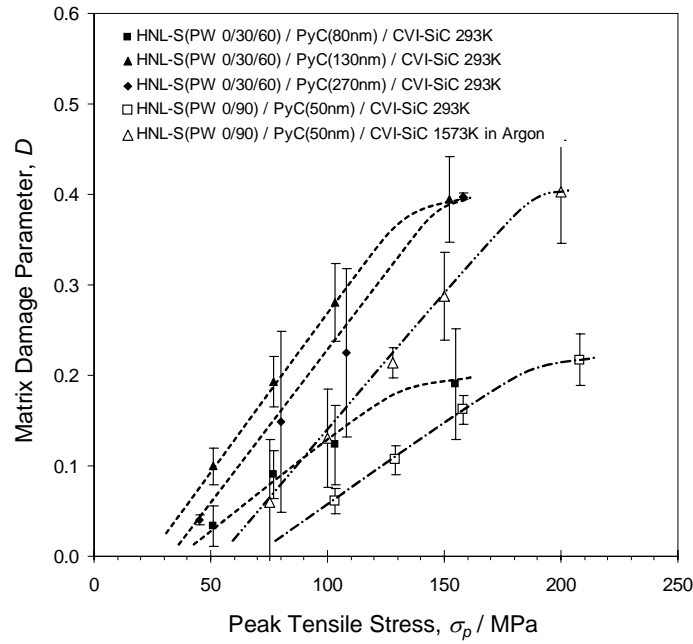


Fig. 9. Peak tensile stress dependence of matrix damage parameter.

where E^* is Young's modulus of the composite with matrix cracks and E_c the initial composite Young's modulus. The matrix damage parameter is approximately proportional to the matrix crack density. The rate of matrix crack accumulation with increasing stress appeared to be significantly different between the composites with nominal interphase thickness of 80nm and those with thickness >120nm. Furthermore, the matrix crack density at composite failure appeared to be significantly lower in the thin interphase materials, including the 0/90 composite, than in the thicker interphase materials. These differences are essential to the apparent dissimilarity seen in stress – strain curves in Fig. 3. The matrix crack accumulation rate at 1573K appeared to be higher than at RT.

Since the matrix crack density in the 0/30/60 composites apparently saturates at slightly below 150MPa of peak stress, as shown in Fig. 3, a linear fit to plots for the peak stress <150MPa intersects the horizontal axis at a matrix cracking stress. Comparison with Fig. 6 confirmed that the matrix cracking stresses at RT agreed well with the average PLS, i.e., 30–35MPa and ~60MPa for the 0/30/60 and 0/90 composites, respectively. The matrix cracking stress at 1573K appeared to be slightly lower than that at RT.

As shown in the inserts of Fig. 8, many of the fiber fracture surfaces exhibited a well-defined hackle and mirror pattern. The fracture strength (σ_f) of each fiber can be estimated using the mirror radius (r_m) measured using the SEM and the following empirical relationship [37].

$$\sigma_f r_m^{1/2} = A_m \quad (2)$$

where A_m is the mirror constant. Taking A_m as 3.5MPa m^{-1/2} [38], the in-situ strength of individual fibers was calculated to be 1.9–2.8GPa with an average of ~2.3GPa, regardless of the interphase thickness or fabric architecture. These numbers are close to the vendor-provided nominal strength (2.6GPa) of Hi-

Nicalon Type-S fibers, which had been measured for fiber bundles. Therefore, the failure of thin interphase composites at a relatively low matrix crack density is not due to the weaker in-situ fiber strength but possibly due to the higher interfacial shear strength.

(2) Hysteresis analysis

In all the hysteresis loops from higher stresses (>75MPa) shown in Fig. 3, each unloading curve consists of an initial parabolic segment followed by a linear segment that continues to <20MPa, and each reloading curve also consists of an initial parabolic segment and the following linear segment that continues until it reaches the stress from which the unloading started. Such behavior can be seen in Fig. 10, in which the reciprocal moduli during the unloading / reloading processes are plotted against stress for three different composites. In the reciprocal modulus plot, the magnitude of the slopes for parabolic unloading and reloading segments are identical in an ideal condition, satisfying the following relationship with the interfacial frictional stress (τ) [39].

$$\left| \frac{d(1/E)}{d\sigma} \right| = \frac{b_2(1-a_1V_f)^2}{2V_f^2\tau E_m} \cdot \frac{r}{d} \quad (3)$$

where V_f is volume fraction of the aligned fibers, E_m the effective mean modulus of matrix, pores, non-aligned fibers and interphase ('inside debonding' is assumed here), r the fiber radius, d the mean matrix crack spacing, and a_1 and b_1 the Hutchinson-Jensen parameters [40]. Figure 10 shows an apparently larger frictional stress in the 56nm-thick interphase composite than in the 178nm-thick interphase composite, if similar matrix crack densities at the given peak tensile stress are assumed. For the majority of the unloading and reloading curves, the slope could be determined with reasonable certainty. For the 0/90 composite, only the slope of the reciprocal reloading modulus could be determined, as was the case for the Tyranno-SA 0/90 composites [33].

As the mean matrix crack spacing was not measured in individual tested specimens, the sliding stress parameter, $\tau/(r/d)$, was defined and plotted in Fig. 11 as a function of interphase thickness. The sliding stress parameters were determined upon both unloading and reloading moduli at peak stress of ~150MPa for the 0/30/60 composites, while they were determined only from the reloading moduli at peak stress of ~200MPa for the 0/90 composite. Plots for the 0/30/60 composites in Fig. 11 indicate a transition of the sliding stress parameter at an interphase thickness of ~100nm. However, the transition is due primarily to the difference in matrix crack spacing, as the matrix damage parameters at the peak stress level of ~150MPa of the 0/30/60 composites with thinner (<100nm) interphases are approximately one half of those of the composites with thicker (>100nm) interphases. Therefore, the influence of interphase thickness on the interfacial sliding stress is not very significant in this range.

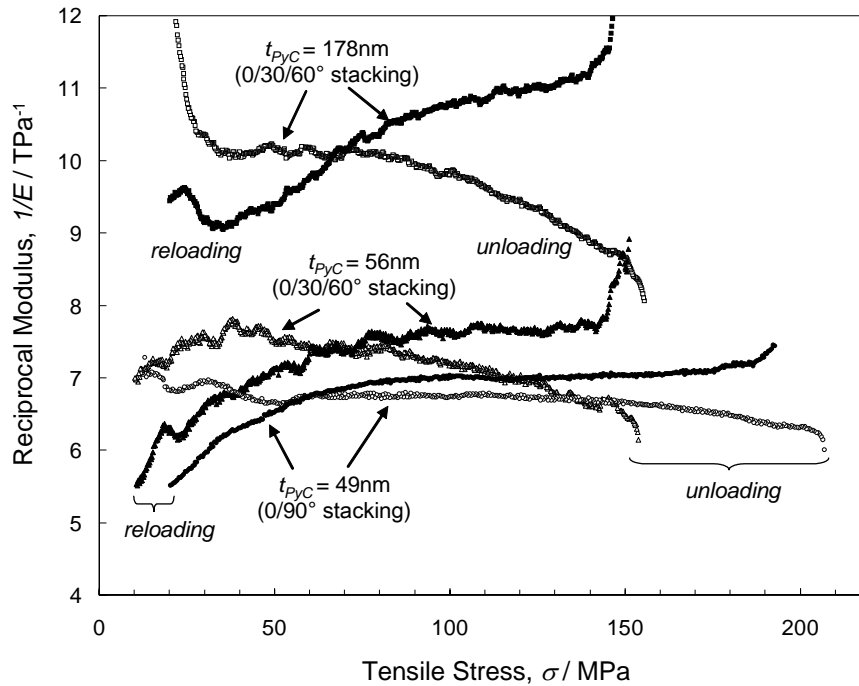


Fig. 10. Reciprocal moduli measured during unloading – reloading sequences incorporated in tensile testing. Material is Hi-Nicalon™ Type-S / PyC (160nm) / CVI-SiC composite.

Transversal matrix cracks in 2D CVI composites initiate mostly at the corners of inter-fiber-bundle pores where a significant stress concentration occurs, thus the saturated crack spacing of one half of the fabric's thread interval can be assumed when the crack initiation in the transversal fiber bundles is neglected. If we assume that is the case and the saturated crack density is achieved at a matrix damage parameter of ~ 0.4 , the interfacial sliding stress τ falls in the range 10 to 20MPa for the composites studied. The sliding stress parameters obtained from the 0/90 composite appeared significantly smaller than those of the 0/30/60 composite with similar interphase thickness, even though the matrix damage parameters (discussed later) were similar at the peak loading stresses applied. This might be attributed to a potential difference in surface conditions between fibers in different generations.

Comparing the sliding stress parameters obtained at 1573K and RT shows a very substantial decrease at the elevated temperature. The same phenomenon is obviously seen in Fig. 4. The absolute values for elevated temperature data points in Fig. 11 are not highly credible due to the low quality of strain data acquisition. However, as the positive drift in strain measurement should have narrowed the hysteresis loops, it is very likely that the much smaller indicated interfacial friction at 1573K is real. The longer fiber pull-out lengths at 1573K also supports this interpretation.

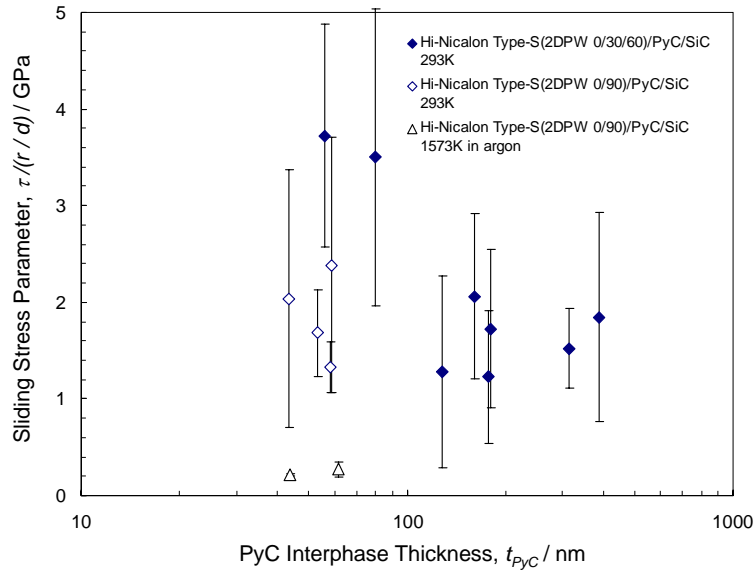


Fig. 11. Influence of PyC interphase thickness on dynamic interfacial sliding stress parameter. Error bars correspond to sum of uncertainty in data interpretation.

(3) Residual stress

The residual thermal stress is inevitable when the coefficients of thermal expansion are different between the fibers and the matrix, as the composites have been cooled down by $>1000\text{K}$ after infiltration. In the Hi-Nicalon Type-S / PyC / CVI-SiC system, the residual stress should be minimal, because the fibers consist primarily of cubic (beta-phase) SiC, that is identical with the matrix constituent. The small amount of excess carbon present in the fiber ($C/Si = 1.05$ according to the specification of the vender) might have affected the thermoelastic properties. Figure 12 presents the residual thermal stress estimated by the method proposed by Vagaggini, et al. [41]. The axial stress in the matrix is approximately comparable to the misfit stress in magnitude and is in tension when the misfit stress is positive. In contrast to the reported positive misfit stress of $\sim+100\text{MPa}$ in a ceramic grade NicalonTM / PyC / CVI-SiC composite [39], the average misfit stress in the present system appeared to be $\sim-20\text{MPa}$. Meanwhile, the extrapolated linear segments of the reloading curves converged at -50 to $+5\text{MPa}$ with an average of $\sim-20\text{MPa}$, suggesting a similar magnitude of axial tensile stress in the matrix. In the ceramic grade Nicalon composite system, the relatively large CTE mismatch between the fibers and matrix can result in a misfit stress as high as a few hundred MPa. The misfit stress can effectively be mitigated by applying a compliant PyC interphase of an appropriate thickness [42]. If that is the case, the measured misfit stress should exhibit negative correlation with the interphase thickness. However, in the Hi-Nicalon Type-S composite system studied, there is no clear correlation between the misfit stress and interphase thickness. This shows that the residual thermal stress in the composite must be insignificant, although a slight positive misfit stress might exist.

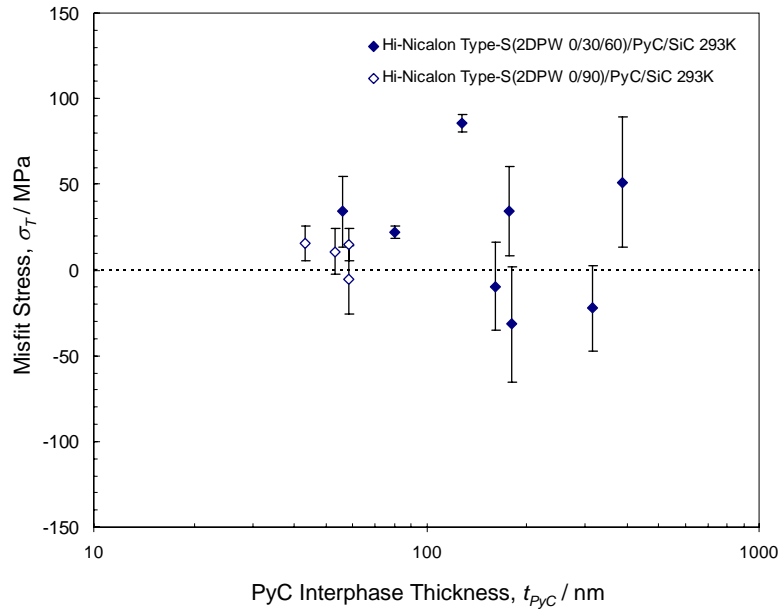


Fig. 12. Thermoelastic misfit stress plotted against PyC interphase thickness for Hi-Nicalon™ Type-S / PyC / CVI-SiC composites. Error bars correspond to sum of uncertainty in data interpretation.

Future Work

The study on PyC interphase thickness effect on tensile properties in the Hi-Nicalon Type-S CVI SiC/SiC composite system is completed. The knowledge obtained in this work have been provided a base in designing the reference SiC/SiC composites for irradiation in HFIR-18J experiment.

References

- [1] R. J. Price, Nucl. Technol. 35 (1977) 320–336.
- [2] G. R. Hopkins, Proceedings of the First Topical Meeting on Technology of Controlled Nuclear Fusion, CONF-740402-P2, Vol. II, San Diego (1974) 437.
- [3] L. L. Snead, S. J. Zinkle, and D. Steiner, J. Nucl. Mater. 191–194 (1992) 560–565.
- [4] G. W. Hollenberg, C. H. Henager, Jr., G. E. Youngblood, D. J. Trimble, S. A. Simonson, G. A. Newsome, and E. Lewis, J. Nucl. Mater. 219 (1995) 70.
- [5] L. L. Snead, Y. Katoh, A. Kohyama, J. L. Bailey, N. L. Vaughn, and R. A. Lowden, J. Nucl. Mater. 283–287 (2000) 551–555.
- [6] Y. Katoh, A. Kohyama, L. L. Snead, T. Hinoki, and A. Hasegawa, Neutron Tolerance of Advanced SiC-Fiber/CVI-SiC Composites, Proceedings of the 19th IAEA Fusion Energy Conference, IAEA-CN-94, International Atomic Energy Agency (2002) FT/P1-03.
- [7] T. Hinoki, L. L. Snead, Y. Katoh, A. Hasegawa, T. Nozawa, and A. Kohyama, J. Nucl. Mater. 307–311 (2002) 1157–1162.
- [8] Y. Katoh, A. Kohyama, T. Hinoki, and L. L. Snead, Fusion Sci. Technol. 44 (2003) 155.
- [9] M. Takeda, J. Sakamoto, A. Saeki, and H. Ichikawa, Ceram. Eng. Sci. Proc. 17 (1996) 35–42.

- [10] T. Ishikawa, Y. Kohtoku, K. Kumagawa, T. Yamamura, and T. Nagasawa, *Nature* 391 (1998) 773–775.
- [11] G. O. Hayner et al., Next Generation Nuclear Plant Materials Research and Development Program Plan, INEEL/EXT-04-02347, Idaho National Engineering and Environmental Laboratory (2004).
- [12] W. R. Corwin, L. L. Snead, S. J. Zinkle, R. K. Nanstad, A. F. Rowcliffe, L. K. Mansur, R. W. Swindeman, W. Ren, D. F. Wilson, T. E. McGreevy, P. L. Rittenhouse, T. Allen, J. Gan, and K. D. Weaver, The Gas Fast Reactor (GFR) Survey of Materials Experience and R&D Needs to Assess Viability (to be published as Oak Ridge National Laboratory Technical Memorandum, U.S. Department of Energy).
- [13] S. Sharafat, F. Najmabadi, and C. Wong, *Fusion Eng. Des.* 18 (1991) 215–222.
- [14] A. S. Perez Ramirez, A. Caso, L. Giancarli, N. Le Bars, G. Chaumat, J. F. Salavy, and J. Szczepanski, *J. Nucl. Mater.* 233–237 (1996) 1257–1261.
- [15] S. Nishio, S. Ueda, I. Aoki, R. Kurihara, T. Kuroda, H. Miura, T. Kunugi, Y. Seki, T. Nagashima, and M. Ohta et al., *Fusion Eng. Des.* 41 (1998) 357–364.
- [16] A. R. Raffray, L. El-Guebaly, S. Gordeev, S. Malang, E. Mogahed, F. Najmabadi, I. Sviatoslavsky, D. K. Sze, M. S. Tillack, X. Wang, and ARIES Team, *Fusion Eng. Des.* 58–59 (2001) 549–553.
- [17] P. Norajitra, L. Buehler, U. Fischer, S. Malang, G. Reimann, and H. Schnauder, *Fusion Eng. Des.* 61–62 (2002) 449–453.
- [18] ARIES Team, M. S. Tillack, X. R. Wang, J. Pulsifer, S. Malang, and D. K. Sze, *Fusion Eng. Des.* 49–50 (2000) 689–695.
- [19] M. Abdou, D. Sze, C. Wong, M. Sawan, A. Ying, and N. Morley, U.S. Plans and Strategy for ITER Blanket Testing, *Fusion Science and Technology* (in press).
- [20] R. J. Price and G. R. Hopkins, *J. Nucl. Mater.* 108–109 (1982) 732–738.
- [21] Y. Katoh, H. Kishimoto, M. Kotani, W. Yang, and A. Kohyama, *J. Nucl. Mater.* 289 (2002) 42–47.
- [22] R. Naslain, *Compos. Sci. Technol.* 64 (2004) 155–170.
- [23] R. A. Lowden, *Ceram. Trans.* 19 (1991) 619–630.
- [24] J. P. Singh, D. Singh, and M. Sutaria, *Compos. A30* (1999) 445–450.
- [25] J. H. Miller, P. K. Liaw, and J. D. Landes, *Mater. Sci. Eng. A* 317 (2001) 49–58.
- [26] W. Yang, H. Araki, T. Noda, J. Park, Y. Katoh, T. Hinoki, J. Yu, and A. Kohyama, *Mater. Trans.* 43 (2002) 2568–73.
- [27] N. Igawa, T. Taguchi, L. L. Snead, Y. Katoh, S. Jitsukawa, A. Kohyama, and J. C. McLaughlin, *J. Nucl. Mater.* 307–311 (2002) 1205–1209.
- [28] T. M. Besmann, J. C. McLaughlin, and H.-T. Lin, *J. Nucl. Mater.* 219 (1995) 31–35.
- [29] K. J. Probst, T. M. Besmann, D. P. Stinton, R. A. Lowden, T. J. Anderson, and T. L. Starr, *Surf. Coat. Technol.* 120–121 (1999) 250–258.
- [30] T. Nozawa, Y. Katoh, A. Kohyama, and E. Lara-Cruzio, Proceedings of the Fifth IEA Workshop on SiC/SiC Ceramic Composites for Fusion Energy Application, International Energy Agency (2002) 74–86.
- [31] T. Nozawa, T. Hinoki, Y. Katoh, A. Kohyama, and E. Lara-Cruzio, Small Specimens Test Techniques: Fourth Volume [ASTM STP 1418, M. A. Sokolov, J. D. Landes, and G. E. Lucas (eds.), ASTM International, West Conshohocken, PA, 2002] 294–305.
- [32] K. Hironaka, T. Nozawa, T. Hinoki, N. Igawa, Y. Katoh, L. L. Snead, and A. Kohyama, *J. Nucl. Mater.* 307–311 (2002) 1093–1097.
- [33] Y. Katoh, T. Nozawa, and L. L. Snead, Mechanical Properties of Thin PyC Interphase SiC-Matrix Composites Reinforced with Near-Stoichiometric SiC Fibers (submitted to *Journal of the American Ceramic Society*).
- [34] A. G. Evans, J.-M. Domergue, and E. Vagaggini, *J. Am. Ceram. Soc.* 77 (1994) 1425–1435.

- [35] W. A. Curtin, *J. Am. Ceram. Soc.* 74 (1991) 2837–45.
- [36] S. Zhu, M. Mizuno, Y. Kagawa, and Y. Mutoh, *Compos. Sci. Technol.* 59 (1999) 833–851.
- [37] J. J. Mecholsky, S. W. Freiman, and R. W. Rice, *J. Mater. Sci.* 11 (1976) 1310–19.
- [38] M. D. Thouless, O. Svaizero, L. S. Sigl, and A. G. Evans, *J. Am. Ceram. Soc.* 72 (1989) 525–532.
- [39] J-M. Domergue, E. Vagaggini, and A. G. Evans, *J. Am. Ceram. Soc.* 78 (1995) 2721–31.
- [40] J. W. Hutchinson and H. M. Jensen, *Mech. Mater.* 9 (1990) 139–163.
- [41] E. Vagaggini, J-M. Domergue, and A. G. Evans, *J. Am. Ceram. Soc.* 78 (1995) 2709–20.
- [42] R. A. Lowden, *Characterization and Control of the Fiber-Matrix Interface in Ceramic Matrix Composites*, ORNL/TM-11039, Oak Ridge National Laboratory (1989).